RMetS
Royal Meteorological Society

Large-eddy simulations of surface influences on planetary boundary layer development in southwest Western Australia

Jatin Kala,[a] Tom J. Lyons,*[a,b] Udaysankar S. Nair[b,c] and Yuling Wu[c]

[a]*Murdoch University, Murdoch, Western Australia, Australia*
[b]*Centre of Excellence for Climate Change Woodland and Forest Health, Murdoch University, Western Australia, Australia*
[c]*Department of Atmospheric Science, University of Alabama in Huntsville, AL, USA*

*Correspondence to: T. J. Lyons, School of Environmental Science, Murdoch University, South Street, Murdoch, WA 6150, Australia. E-mail: t.lyons@murdoch.edu.au

Observations from near-simultaneous atmospheric soundings released over contrasting land surfaces in the southwest of Western Australia during December 2005 (austral summer) and August 2007 (late austral winter or early spring) have shown higher planetary boundary layer (PBL) heights over native vegetation as compared to agricultural land. The large-eddy simulation technique is used to investigate the drivers behind these observed differences in PBL, and sensitivity tests are carried out with modified soil moisture and vegetation cover. It is shown that the differences in PBL for the December case are mainly driven by the change in vegetation cover, while a soil moisture gradient also played a role for the August case. The mixing diagram approach is used to further quantify the relative contributions of surface and entrainment fluxes on the growth of the PBL and it is shown that, while dry-air entrainment plays an important role in PBL development, it is the higher surface Bowen ratio which drives the more vigorous PBL development over the native vegetation. It is also shown that the enhanced PBL development over the native vegetation leads to the preferential formation of shallow convective clouds for the August case.

Key Words: land–atmosphere interactions; large-eddy simulations; planetary boundary layer; Regional Atmospheric Modeling System

Received 01 July 2011; Revised 20 November 2011; Accepted 14 December 2011; Published online in Wiley Online Library 1 February 2012

Citation: Kala J, Lyons TJ, Nair US, Wu Y. 2012. Large-eddy simulations of surface influences on planetary boundary layer development in southwest Western Australia. *Q. J. R. Meteorol. Soc.* **138**: 1465–1475. DOI:10.1002/qj.1879

1. Introduction

The southwest of Western Australia (SWWA) is a region of extensive land cover change, with an estimated 13 million hectares of native vegetation cleared since the European settlement (Huang *et al.*, 1995). This is illustrated in Figure 1 showing the vermin fence acting as a clear boundary between native vegetation east of the fence, and agricultural land use west of the fence (shaded). The impacts of such an extensive change in land use have been investigated via a series of ongoing micro-climatological field experiments (*BuFex*) (Lyons *et al.*, 1993; Nair *et al.*, 2011), using a combination of aircraft and satellite data as well as standard meteorological sensors. The aircraft data have shown higher averaged sensible heat fluxes over the native vegetation due to the reduced albedo, higher surface roughness and canopy resistance, and higher latent heat fluxes over the agricultural crops due to higher transpiration during winter (Lyons *et al.*, 1993).

Higher sensible heat fluxes imply a more developed convective boundary layer; however, the data of Lyons *et al.* (1993) were over a temporal scale of days, and their results cannot easily be generalized. As such, Huang *et al.* (1995) used a combination of satellite data and a one-dimensional soil–vegetation boundary layer model (Huang and Lyons, 1995) to show that sensible heat fluxes are

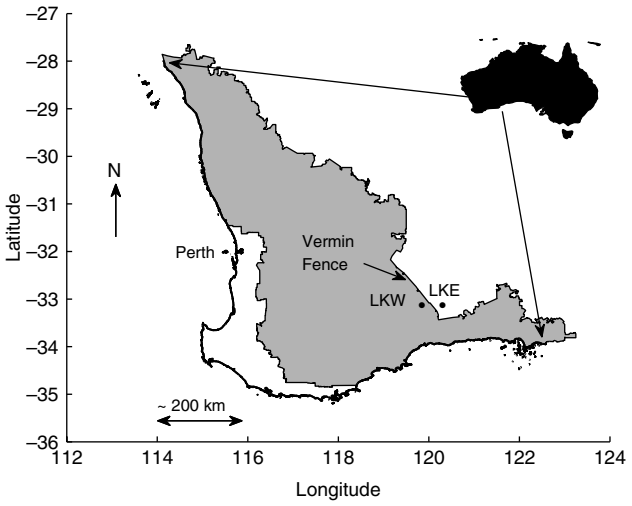

Figure 1. Map showing the vermin fence acting as a boundary between agricultural land use (shaded), west of the fence, and native vegetation, east of the fence, in southwest Western Australia (SWWA). The map shows the release locations of the NCAR atmospheric soundings at Lake King East (LKE) and Lake King West (LKW).

consistently higher over the native vegetation throughout the year, while latent heat fluxes are higher over the agricultural region during the growing season. Their one-dimensional boundary layer model showed planetary boundary layer (PBL) heights to be consistently higher over the native vegetation and above the lifting condensation level (LCL) during spring and summer months. Lyons (2002) further expanded on the work of Huang *et al.* (1995) using the same one-dimensional boundary layer model to show that a deeper PBL over the native vegetation leads to the preferential formation of convective clouds over this region through a moistening of the upper PBL. While these simulations highlight the role of the surface, the effect of the spatial inhomogeneity has been further reinforced by large-eddy simulations (LES) of the boundary effects of the abrupt change in land use at the fence, which have shown the formation of roll-like circulations resulting in significant horizontal heat and moisture flux (Esau and Lyons, 2002). These rolls are estimated to accumulate up to 30% of the water evaporated within a 5 km strip of the agricultural area. Pitman *et al.* (2004) further expanded on the work of Lyons (2002) by using a three-dimensional mesoscale atmospheric model to investigate the impacts of land cover change on the July climate of SWWA. They showed that the decrease in precipitation can be partly explained by a decrease in low-level moisture convergence due to a change in surface roughness. More recent investigations based on individual case studies have shown that the replacement of native vegetation with agriculture results in a decrease in convective precipitation associated with cold fronts and the west coast trough (a synoptic feature which initiates summer and springtime convection in SWWA), due to a decrease in turbulent kinetic energy and moisture convergence, and an increase in wind speeds within the lower boundary layer (Kala *et al.*, 2011; Nair *et al.*, 2011).

Similar studies have been conducted elsewhere. Doran *et al.* (1995) investigated boundary layer characteristics over areas of inhomogeneous surface fluxes, namely a semiarid grassland steppe and an irrigated farmland. They found that on days with lighter winds a thermal circulation can be set up related to the thermal contrast between the two areas, analogous to a sea breeze circulation. Ek and Holtslag (2004) investigated the effects of soil moisture on the boundary layer using a one-dimensional coupled land surface boundary layer model. They found that soil moisture has the potential to promote cloud development above the PBL provided there is sufficient instability above; sufficient initial humidity within the PBL; and that the air above the PBL is not too dry. They also found that when stability above the PBL is weak dry soil (low soil moisture) can result in higher PBL relative humidity tendency and hence cloud cover. Santanello *et al.* (2005) investigated the relationships between PBL development and land surface conditions using radiosonde and surface flux data over the US southern Great Plains. They found that 76% of the variance in PBL height can be explained by atmospheric stability in the layer of PBL growth, as well as soil water content. Santanello *et al.* (2007) combined the observations of Santanello *et al.* (2005) with a single-column PBL/land surface model to further investigate the feedbacks. While their results further reinforced the findings of Santanello *et al.* (2005), they also found that adequate parametrizations of entrainment and the residual mixed layer are critical in quantifying PBL growth. Similar results have been found by van Heerwaarden *et al.* (2009); namely that under certain conditions the convective boundary layer (CBL) height is not only responsive to land surface properties but also to dry-air entrainment of free tropospheric air into the CBL. As such, Santanello *et al.* (2009) have devised a framework for quantifying land–atmosphere feedbacks based on mixing diagrams (Betts, 1992) which include a surface vector flux as well as an entrainment vector, providing a complete assessment of land–atmosphere feedbacks. Recent work by Wang *et al.* (2010) on the properties of a simulated boundary layer over inhomogeneous vegetation have shown that the effects of surface heterogeneity remain significant with geostrophic winds of up to 10 m s^{-1} and, under the right conditions, two-dimensional strips of alternating soil and vegetated surfaces can favour the initiation of deep convection. Their simulations, however, remain highly idealized.

The latest *BuFex* field campaign recently completed the collection of atmospheric soundings at either side of the vermin fence near the town of Lake King, at Lake King East (LKE) and Lake King West (LKW) respectively (Figure 1) during December 2005 (summer) and August 2007 (spring or late winter). An initial analysis of these near-simultaneous soundings have shown enhanced PBL development over the native vegetation at LKE as compared to agricultural land or bare soil at LKW on several days (Nair *et al.*, 2011). The largest differences observed were on the 17 December 2005 at 1500 h (0700 UTC) and 21 August 2007 at 1200 h (0400 UTC), which were characterized by a large anticyclonic cell with low pressure gradient and accompanying clear and calm conditions, providing ideal conditions to detect changes in PBL due to land surface influences. While previous studies have already suggested mechanisms behind the enhanced boundary layer development over the native vegetation, these have been based on highly idealized LES (Esau and Lyons, 2002), limited to one-dimensional models (Huang *et al.*, 1995; Lyons, 2002), or the spatial resolution of the three-dimensional numerical models used were too large to investigate boundary layer processes in adequate detail (Kala *et al.*, 2011; Nair *et al.*, 2011). Moreover, on the case study days considered by Lyons (2002), air above the PBL was too moist for dry-air entrainment, and the

relative importance of surface *versus* entrainment fluxes on the development of the PBL in SWWA remains largely unexplored. Accordingly, the aim of this paper is to investigate the surface influences driving these differences in boundary layer dynamics. LES are carried out using the Regional Atmospheric Modeling System (RAMS) version 6.0 and the model is evaluated against the soundings. Sensitivity tests are then carried out with different soil moisture initialization and vegetation cover and the mixing diagram approach is applied to quantify the surface and entrainment fluxes.

2. Study area and field data

SWWA is characterized by a Mediterranean climate with warm, dry summers and cool, wet winters (Gentilli, 1971). Field observations were undertaken in December 2005 and August 2007. December is during the austral summer season, with the agricultural region being bare of crops following harvest and covered with harvest stubble approximately 0.2 m high or bare soil; August is during late winter to early spring, with the agricultural region active. The native vegetation east of the fence (Figure 1) is undisturbed and in its pristine state. It is mostly comprised of *Eucalyptus eremophilia* species, and patches of eucalypt woodland can be found on the lower ground and *Casuarina* thickets on the residual plateau soils (Lyons *et al.*, 1996). The height of the native trees varies between 0.5 and 6.0 m and more than 75% are between 0.5 and 2.0 m high (Esau and Lyons, 2002). There is no irrigation across the region and the overall landscape inland is flat. The predominant soil type is a duplex soil of sand over clay.

High-resolution atmospheric soundings were acquired using the National Center for Atmospheric Research (NCAR) Mobile Global Positioning Advanced Upper-Air Sounding System during the first three weeks of December 2005 and August 2007 at 3-hourly intervals at two locations approximately 45 km apart near the town of Lake King, namely the Lake King West (LKW) and Lake King East (LKE) sites respectively (Figure 1). The soundings provided profiles of temperature, relative humidity, wind speed and direction either side of the vermin fence (i.e. the LKW site in the agricultural region and the LKE site in the native vegetation) from the surface to about 12 km. These data were collected as part of the ongoing *BuFex* field campaign (Lyons *et al.*, 1993) and all soundings were subjected to NCAR data quality control. The morning soundings were used to initialize the model and the afternoon soundings were used for model evaluation (not assimilated).

3. Model description and initialization

RAMS is a highly versatile three-dimensional mesoscale meteorological model (Pielke *et al.*, 1992; Cotton *et al.*, 2003) that has been extensively used for a wide variety of applications, including LES (Avissar *et al.*, 1998; Eastman *et al.*, 1998; Avissar and Schmidt, 1998; Gopalakrishnan *et al.*, 2000; Gopalakrishnan and Avissar, 2000; Cheng *et al.*, 2001; Bohrer *et al.*, 2009; Angevine *et al.*, 2010). The latest 6.0 version was utilized and operated as a non-hydrostatic, compressible, primitive equation model with a σ_z terrain-following vertical coordinate system with polar stereographic coordinates. RAMS 6.0 is coupled to a Land Ecosystem–Atmosphere Feedback Model (LEAF-3), which represents the energy and moisture budgets at the surface and their interactions with the atmosphere (Walko *et al.*, 2000). It incorporates the interactions between soil and vegetation and the atmosphere at a subgrid scale; see Walko *et al.* (2000) for detailed model descriptions.

The model grid domain was centred between the LKW and LKE sites (Figure 1) and covered an area 100 × 40 km, such that both sites were in the domain and not too close to the grid boundaries. In order to adequately simulate the observed differences in PBL between the two sites (a few hundred metres), 160 vertical levels were used, with the lowest level being 20 m above the ground, and subsequent levels stretched by a factor of 1.15 to a maximum of 25 m, after which all levels were 25 m higher than the previous. The horizontal grid spacing used in LES studies of the PBL typically varies from 100 m (e.g. Avissar *et al.*, 1998; Cheng *et al.*, 2001) to 500 m (e.g. Tian *et al.*, 2003; Wang *et al.*, 2010). Given the large domain size and high vertical resolution used, a horizontal grid spacing of 250 m was found to be both adequate in simulating the observed differences in PBL at both sites as well as being computationally efficient. While a grid spacing of 250 m is not ideal for resolving the fine spatial structure of turbulence associated with large eddies, a grid spacing of 500 m or less is adequate for resolving convective structures within the PBL (Tian *et al.*, 2003), which is of interest to this study.

The model was homogeneously initialized with the mean of the LKW and LKE morning soundings at 0900 h (0100 UTC) for the 17 December 2005 case and 0600 h (2200 UTC) for the 21 August 2007 case, and integrated for 12 h. (We note that there were no major differences in the morning soundings at the two sites, and the different initialization times for the two case studies are due to the availability of soundings at different times.) The Harrington scheme (Harrington, 1997) was used for long-wave and short-wave radiation, which is the most sophisticated option available in RAMS, and explicit cloud microphysical parametrization was activated (see Walko and Tremback, 2006). The 1.5-order closure scheme of Deardorff (1980) was used for subgrid-scale turbulence; cyclic conditions were used for lateral boundary conditions; and a rigid lid was used as the top boundary condition, with a Rayleigh friction scheme applied to the top eight layers to absorb spurious gravity waves and reduce reflection from the upper part of the simulated domain. The soil–vegetation model was activated for all runs and the vegetation biophysical parameters (albedo, fractional vegetation cover and minimum stomatal resistance) were changed to monthly values published in Huang *et al.* (1995) to better reflect the growing stage of the native vegetation and crop for December and August. This study used the same input geographical datasets as described in Kala *et al.* (2011), including 9s (∼250 m) topography (Hutchinson *et al.*, 2009) and the Australian Surveying and Land Information Group (AUSLIG) current and pre-European (undisturbed) vegetation datasets (AUSLIG, 1990).

Three experiments were carried out as summarized in Table 1. The control experiments (CNTL) were used to evaluate the model's performance in reproducing the observed differences in PBL for the two case studies. These experiments used the AUSLIG data for current vegetation conditions, except that crops were replaced with bare soil for the 17 December simulation since the harvest was completed by then. Soil moisture initialization was carried out using

Table 1. Summary of numerical experiments.

Experiment name	Vegetation cover	Soil moisture initialization
CNTL	Current	AWAP
CNTL-CM	Current	Constant
PRE-EU	Pre-Eu	Constant

the Australian Soil Water Availability Project (AWAP) (Raupach *et al.*, 2008, 2009) soil moisture products. These data provide monthly means of upper (surface to 0.2 m) and lower (0.2–1.5 m) relative soil moisture (percentage of field capacity) across the Australian continent at a 5 × 5 km grid spacing. A two-week spin-up was carried out using the AWAP data and following the same model specifications as described in Kala et al. (2011), except that a fourth nested grid was used to obtain a resolution of 1 km. The soil moisture and soil temperature output from this spin-up run was then interpolated to the 250 m LES grid. This ensured a realistic representation of initial soil conditions, which are well documented to have a strong influence on the PBL (e.g. Ek and Holtslag, 2004).

In order to investigate the influence of vegetation cover and soil moisture on the PBL, tests were carried out with horizontally homogeneous soil moisture initialization (CNTL-CM), and with pre-European vegetation cover (PRE-EU). The CNTL-CM experiment is the same as CNTL except that a horizontally homogeneous dry soil moisture profile is used with the soil moisture estimates obtained from Li and Lyons (2002). The PRE-EU experiment is the same as CNTL-CM except that the vegetation type at LKE (wooded grasslands) is used throughout the domain. It is noted that we did not use the AWAP soil moisture dataset to carry out a separate spin-up for the PRE-EU experiment as this soil moisture product is representative of current vegetation conditions. It is also noted that several studies investigating surface influences on the PBL carry out experiments with saturated *versus* completely dry soils (e.g. Findell and Eltahir, 2003a, 2003b; Ek and Holtslag, 2004). We do not carry such experiments here as saturated soil profiles are rare in this semiarid region but, rather, focus on understanding the impacts of land cover change.

4. Model evaluation

The observed and simulated differences in PBL depth on 17 December 2005 and 21 August 2007 are shown in Figures 2 and 3 respectively. The observed soundings clearly show higher PBL heights over the native vegetation by about 500 m and 250 m for the December and August cases respectively (ΔPBL in Figures 2(a) and 3(a)), which is also evident in the profiles of specific humidity (Figures 2(b) and 3(b)) (the different times for each case study correspond to times when the observed differences in PBL between the two sites were largest). The differences are reasonably well reproduced by the model (CNTL experiments) with the simulated profiles of potential temperature within 1–2 K

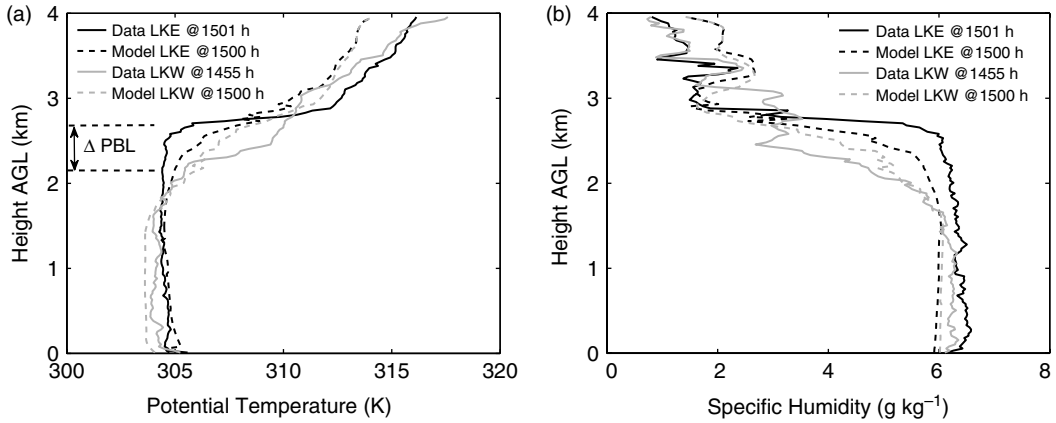

Figure 2. Observed and simulated vertical profiles of (a) potential temperature (K) (b) and specific humidity (g kg^{-1}) at the LKW and LKE sites (Figure 1) at 1500 h (0700 UTC) on 17 December 2005.

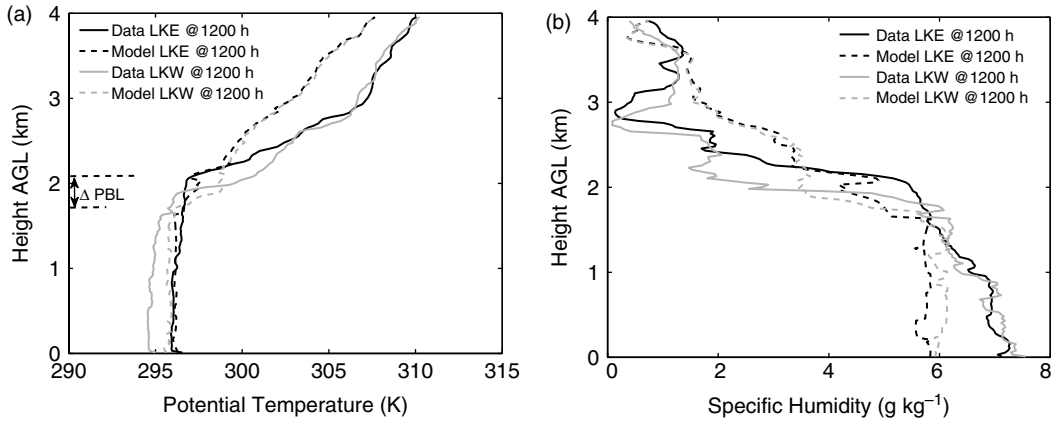

Figure 3. Same as in Figure 2 except at 1200 h (0400 UTC) on 21 August 2007.

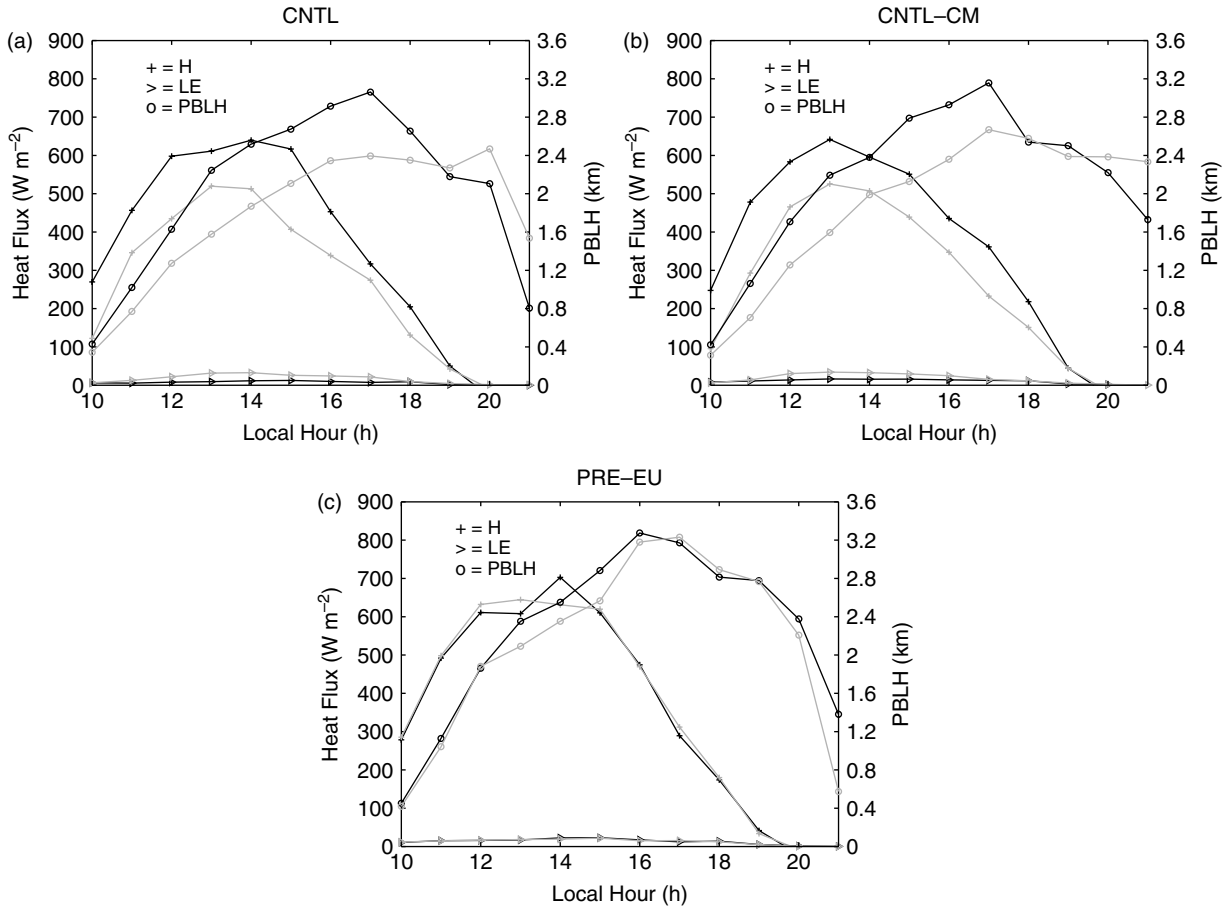

Figure 4. Temporal evolution of the surface sensible (H) and latent (LE) heat fluxes (W m^{-2}) and height of the PBL (PBLH) (km) from 1000 h (0200 UTC) to 2100 h (1300 UTC) on 17 December 2005 at the LKE (black) and LKW (grey) sites.

and specific humidity within 1–2 g kg^{-1} of the observations. The simulated differences in PBL are smaller as compared to the observed differences but, nonetheless, the simulations reproduce the overall qualitative trends.

The magnitude of the differences between the observed and simulated profiles are consistent with the RAMS-LES study by Avissar *et al.* (1998), who report their simulated profiles of potential temperature and specific humidity to be within 1 K and 1 g kg^{-1} of the observations. However, Avissar *et al.* (1998) carried out several iterations using artificial profiles, until the simulated profiles corresponded to observed profiles at a later time; imposed surface flux observations on the model; and did not activate cloud microphysical processes or the land surface scheme (these model settings were reasonable given their aims). Hence the results shown here are quite encouraging as we did not impose such constraints on the model but relied on the land surface and atmospheric parametrization schemes.

5. Results and discussion

Having sufficient confidence in the model's ability to reproduce the differences in PBL between the two sites, we now examine the influence of vegetation type and soil moisture on the PBL. This is illustrated in Figure 4 showing the time series of average surface sensible and latent heat flux and PBL heights (the height above the surface at which the turbulent kinetic energy becomes close to zero) for each experiment (Table 1) for the December (summer) case. Figure 4(a) shows higher sensible heat fluxes over the LKE site (native vegetation) as compared to the LKW site (bare soil in December) for the CNTL experiment, with the latent heat fluxes being close to zero at both sites. The fluxes simulated by the model are consistent with recent observations (Nair *et al.*, 2011) but significantly lower than those observed in the earlier *BuFex* experiments (Lyons *et al.*, 1993). The long-term AWAP soil moisture analysis (Raupach *et al.*, 2008, 2009) shows a considerable drying out of the topsoil over this period, which has undoubtedly contributed to the lower latent fluxes observed. The higher sensible heat flux at LKE is due to the lower albedo and higher stomatal resistance of the native vegetation (Lyons *et al.*, 1993; Huang *et al.*, 1995; Lyons, 2002), and this corresponds to higher PBL heights throughout the day. Running the model with a horizontally homogeneous soil moisture profile (Figure 4(b)) resulted in very similar results to the CNTL experiment (Figure 4(a)), with the mean difference in PBL height and sensible heat flux between LKE and LKW sites between the CNTL and CNTL-CM experiments (i.e. $\Delta\mathrm{PBL}_{\mathrm{CNTL}} - \Delta\mathrm{PBL}_{\mathrm{CNTL\_CM}}$ and $\Delta H_{\mathrm{CNTL}} - \Delta H_{\mathrm{CNTL\_CM}}$) being 0.5 m and 1.9 W m^{-2} respectively. This shows that the differences in PBL height are driven by a change in vegetation cover, rather than a soil moisture gradient between the two sites. This is further confirmed by Figure 4(c), showing no distinct difference in sensible and latent heat fluxes and PBL heights when pre-European vegetation is used throughout the domain.

Figure 5 is the same as Figure 4, except for the August (late winter) case. Figure 5(a) shows higher sensible heat

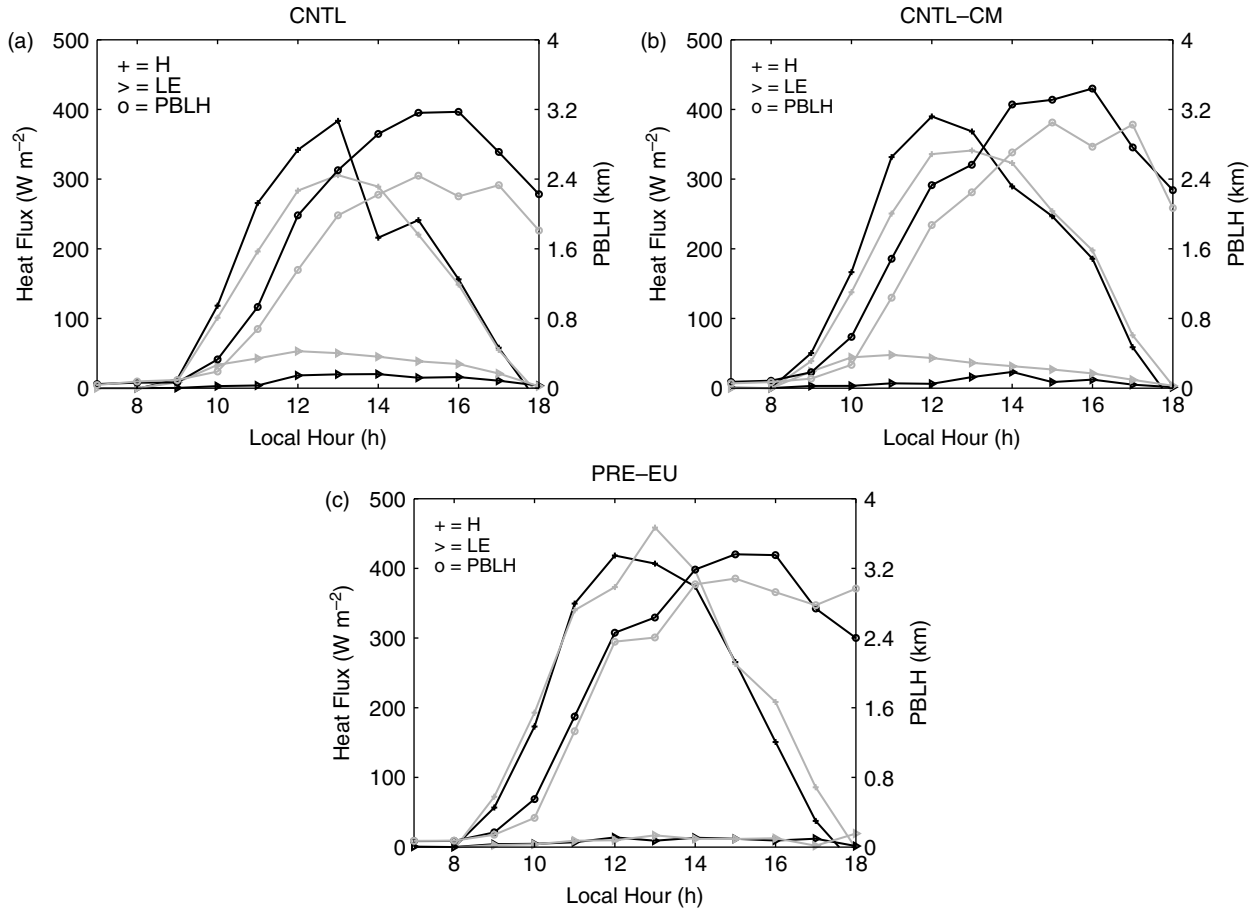

Figure 5. Same as in Figure 4 except from 0700 h (2300 UTC) to 1800 (1000 UTC) on 21 August 2007.

fluxes and PBL heights and lower latent heat fluxes over the LKE site (native vegetation) as compared to the LKW site (crops in August). The higher latent heat fluxes over the LKW site are due to higher transpiration from crops at this location as compared to the native vegetation, which has a higher minimum stomatal resistance, consistent with previous research (Lyons *et al.*, 1993; Huang *et al.*, 1995; Lyons, 2002). A notable feature in Figure 5(a) is the sharp decrease in sensible heat flux from 1300 to 1400 h by almost 180 W m^{-2} at the LKE site. This corresponded to a decrease in incoming short-wave radiation (not shown), due to the formation of clouds as illustrated in Figure 6(a), showing the cloud water mixing ratio at 1300 h (2100 UTC) at 2405 m above ground level for the CNTL experiment. There is a preferential formation of shallow cumulus clouds on the east side of the grid (native vegetation) as compared to the west side (crops), consistent with the aircraft observations of Lyons *et al.* (1993) and satellite observations of Ray *et al.* (2003). This is further confirmed by visible satellite imagery shown in Figure 7. At 1000 h (0200 UTC), there are no clouds either side of the vermin fence, but a large synoptically driven cloud band can be seen in the west, moving east. At 1100 h (0300 UTC), thin cloud bands are observed east of the fence, which develop into parallel bands at 1200 h (0400 UTC). By 1300 h (0500 UTC), the large cloud band to the west has moved over the fence.

Running the model with a horizontally homogeneous soil moisture profile (Figure 5(b)) resulted in the difference in PBL heights between LKE and LKW being smaller as compared to the CNTL case (Figure 5(a)); namely, the mean difference in PBL height between the two sites between the CNTL and CNTL-CM experiment was 135.4 m. This is the result of a soil moisture gradient as illustrated in Figure 8, showing the average surface (top three layers) soil moisture for the CNTL experiment. The soil moisture was higher on the west side of the grid, resulting in less of the available energy being partitioned into sensible heat, and hence lower PBL height. This soil moisture gradient is due to the AWAP soil moisture data used for soil moisture initialization having an east–west gradient in soil moisture as rainfall during winter months decreases from west to east due to the regular passage of frontal systems. In contrast, the surface soil moisture for the CNTL-CM experiment (not shown) was homogeneous at approximately 0.05 m m^{-3} throughout the grid. Hence the difference in PBL heights for the August case is the result of both vegetation cover and a soil moisture gradient. It is also clear when comparing Figure 6(a) and (b) that the soil moisture gradient (CNTL experiment) results in enhanced formation of clouds over the native vegetation as compared to uniform drier soil moisture (CNTL-CM experiment). This is further confirmed in Figure 5(c) showing no distinct difference in heat fluxes and PBL height between the two sites for the PRE-EU experiment, with nearly uniform cloud formation throughout the domain (Figure 6(c)).

In summary, the results presented here are consistent with Lyons *et al.* (1993), Huang *et al.* (1995), Lyons (2002), and Nair *et al.* (2011). Namely, the native vegetation east of the vermin fence, with its lower albedo and higher stomatal

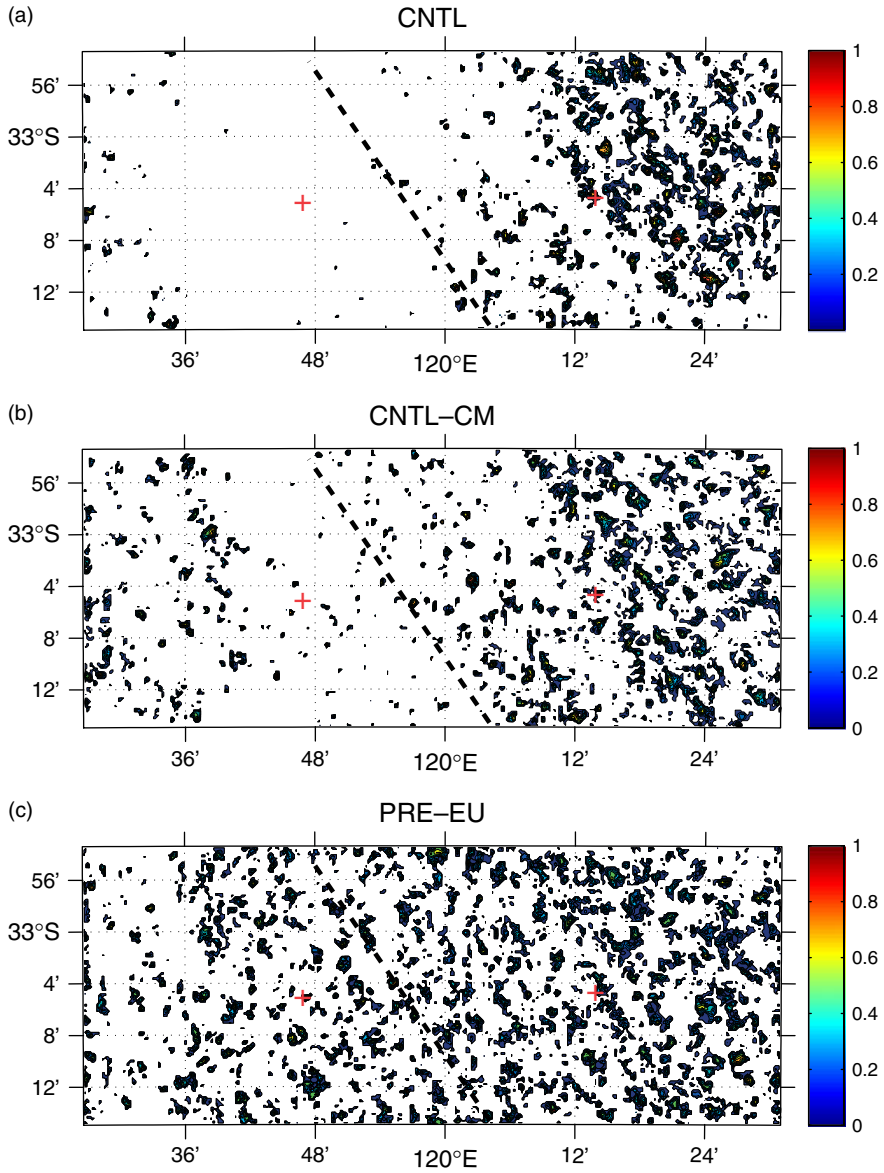

Figure 6. Cloud water mixing ratio (g kg^{-1}) at 1300 h (2100 UTC) at 2405 m above ground level for the August simulations. The crosses are the locations of LKW (left) and LKE (right) respectively and the black dotted line represents the boundary between the native vegetation and crops. This figure is available in colour online at wileyonlinelibrary.com/journal/qj

resistance, results in higher sensible heat fluxes, which promotes the formation of a deeper PBL and higher chances of convective cloud formation. However, the analysis so far neglects to account for the role of entrainment fluxes which can influence the growth of the PBL (e.g. Santanello *et al.*, 2005; van Heerwaarden *et al.*, 2009). In order to account for these, we apply the mixing diagram theory of Betts (1984, 1992), which uses a vector representation of the diurnal co-evolution of temperature and humidity to quantify the heat and moisture budgets in the PBL. The mixing diagram theory has been successfully applied by Santanello *et al.* (2009) to quantify local land–atmosphere feedbacks in the US southern Great Plains, using both numerical simulations and observations. The full derivation and discussion of the theory can be found in Betts (1992).

As discussed in Santanello *et al.* (2009), the evolution of the near-surface potential temperature (θ) and specific humidity (q) is sensitive to, and integrative of, land–atmosphere processes. Hence the latter can be represented in vectorial form by plotting the evolution of θ and q in energy terms (i.e. Lq *versus* $C_p\theta$, where L is the latent heat of vaporization and C_p the specific heat), and the entrainment and surface vectors can be computed using the initial and final values of θ and q (at ≈ 2 m), as well as the mean surface energy fluxes and PBL height during these times. For example, the surface vector for heat is defined as (Santanello *et al.*, 2009):

$$C_p \Delta\theta_{\mathrm{sfc}} = \frac{\overline{H_{\mathrm{sfc}}}\Delta t}{\rho_{\mathrm{m}}\mathrm{PBLH}}, \qquad (1)$$

where $\overline{H_{\mathrm{sfc}}}$ and $\overline{\mathrm{PBLH}}$ are the mean sensible heat flux and PBL heights respectively over the time step Δt , and ρ_{m} is the density in the mixed layer.

The entrainment vector is then the residual that connects the surface vector for heat and moisture to the final values of $C_p\theta$ and Lq, scaled by a volume defined by PBLH. This is illustrated in Figures 9 and 10, showing the mixing diagrams for each experiment (Table 1) for the December and August cases respectively, with the respective energy budgets shown

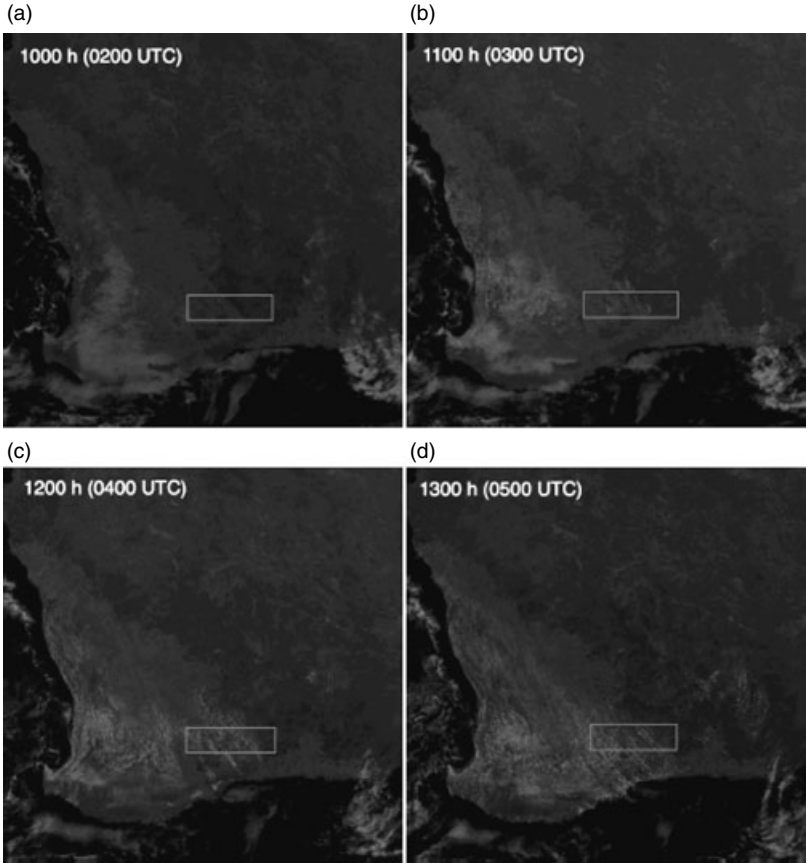

Figure 7. Visible channel imagery over SWWA on 21 August 2007 from the Multifunction Transport Satellite (MTSAT) at (a) 1000 h (0200 UTC), (b) 1100 h (0300 UCT), (c) 1200 h (0400 UTC) and (d) 1300 h (0500 UTC).

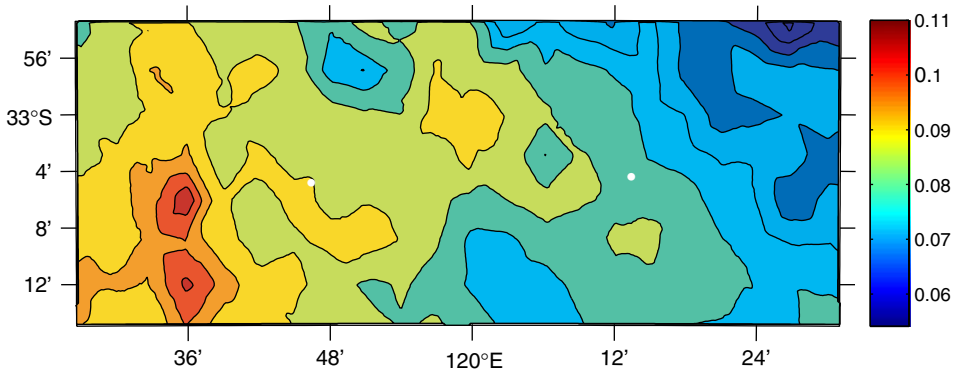

Figure 8. Average surface (top three layers) soil moisture ($m^3\ m^{-3}$) for the CNTL experiment for the August case. The white dots are the locations of LKW (left) and LKE (right) respectively. This figure is available in colour online at wileyonlinelibrary.com/journal/qj

in Tables 2 and 3. β_{sfc} and β_{ent} are the surface and entrainment Bowen ratios respectively (i.e. $\beta_{sfc} = H_{sfc}/LE_{sfc}$ and $\beta_{ent} = H_{ent}/LE_{ent}$), and their vector representation is shown as the slope of the dotted lines emanating from the start and end values of Lq and $C_p\theta$. A_h and A_{le} are the ratio of the sensible and latent heat of entrainment to that of the surface respectively (i.e. $A_h = H_{ent}/H_{sfc}$ and $A_{le} = LE_{ent}/LE_{sfc}$).

We first examine the overall shape of the $Lq - C_p\theta$ curves for the December case (Figure 9). There is clearly little evaporation from the surface (i.e. no clear increase in Lq during the day) for all three experiments, which is expected due to dry soil conditions, consistent with the mixing diagrams of Santanello *et al.* (2009) for their dry-soil experiments. The curves for the CNTL and CNTL-CM experiments (Figure 9(a, b)) also show that the LKE site was slightly warmer and drier for the first 3–4 hours as compared to the LKW site. This can be contrasted with the curves for the PRE-EU experiment showing no difference between the two sites. The large and negative values of β_{ent} indicate that dry-air entrainment was a dominant process at both sites for all three experiments. However, while β_{ent} was the same order of magnitude at both sites for all experiments, β_{sfc} was at least twice as high at LKE as compared to LKW for the CNTL and CNTL-CM experiments, but similar for the PRE-EU experiment. This is also clear in Table 2 showing that the main difference between LKE and LKW for the CNTL and CNTL-CM experiments is in H_{sfc}, rather than H_{ent}. It is noted that the magnitudes of β_{sfc} are much higher as compared to those in Santanello *et al.* (2009). This is because the magnitude of LE_{sfc}

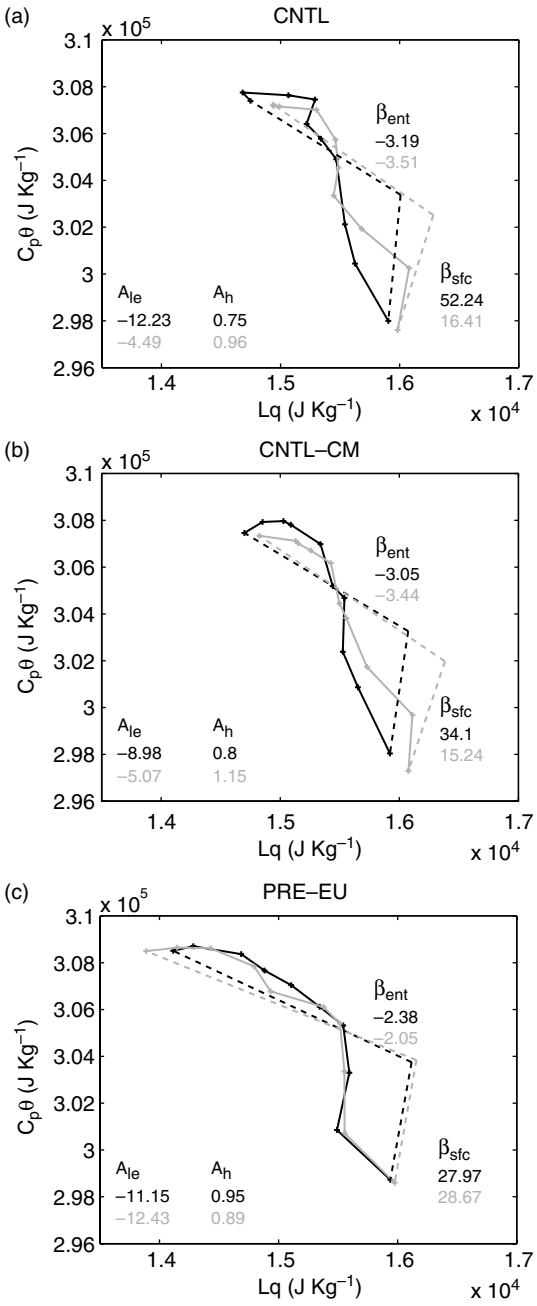

Figure 9. Co-evolution of Lq and $C_p\theta$ on 17 December 2005 at LKE (black) and LKW (grey) using the mixing diagram approach.

is small. A_h was close to one for all experiments at both sites, showing that there was little difference between H_{sfc} and H_{ent} (Table 2), but A_{le} was higher at LKE for the CNTL and CNTL-CM experiments. This is because LE_{sfc} was almost twice as low at LKE (wooded grasslands) as compared to LKW (bare soil). Similar trends were found for the August case (Figure 10 and Table 3). Namely, the overall shapes of the $Lq - C_p\theta$ curves show that the LKE site was slightly warmer and drier as compared to LKW during the first 3–4 hours, B_{ent} was large and negative, but the same order of magnitude at both sites, β_{sfc} and A_{le} were higher at LKE as compared to LKW for the CNTL and CNTL-CM experiments, but similar for the PRE-EU experiment, and A_h was the same order of magnitude at both sites. However, there were also some differences, namely, β_{sfc} was at least four times higher at LKE as compared to LKW (compared with twice for the December case). This can be explained by the fluxes in Table 3 showing that LE_{sfc} at LKE was at least three times as small as compared to LKW for the August case, as compared to only twice as small for the December case (Table 2). The higher LE_{sfc} at LKW during August as compared to December is due to having transpiring crops at LKW in August, as compared to bare soil. An interesting observation is that LE_{ent} at LKE for the PRE-EU experiment was higher as compared to LE_{ent} at LKE for the CNTL experiment (although the LKE site has wooded grasslands for both experiments). This is because the mean PBL at LKE for the PRE-EU experiment was higher as compared to the CNTL experiment due to the different soil moisture and temperature initialization used for two experiments.

In summary, the mixing diagrams show that, while dry-air entrainment was an important process for all the experiments (large and negative β_{ent}), it is the higher β_{sfc} at LKE which drives the higher PBL heights at this site, i.e. the

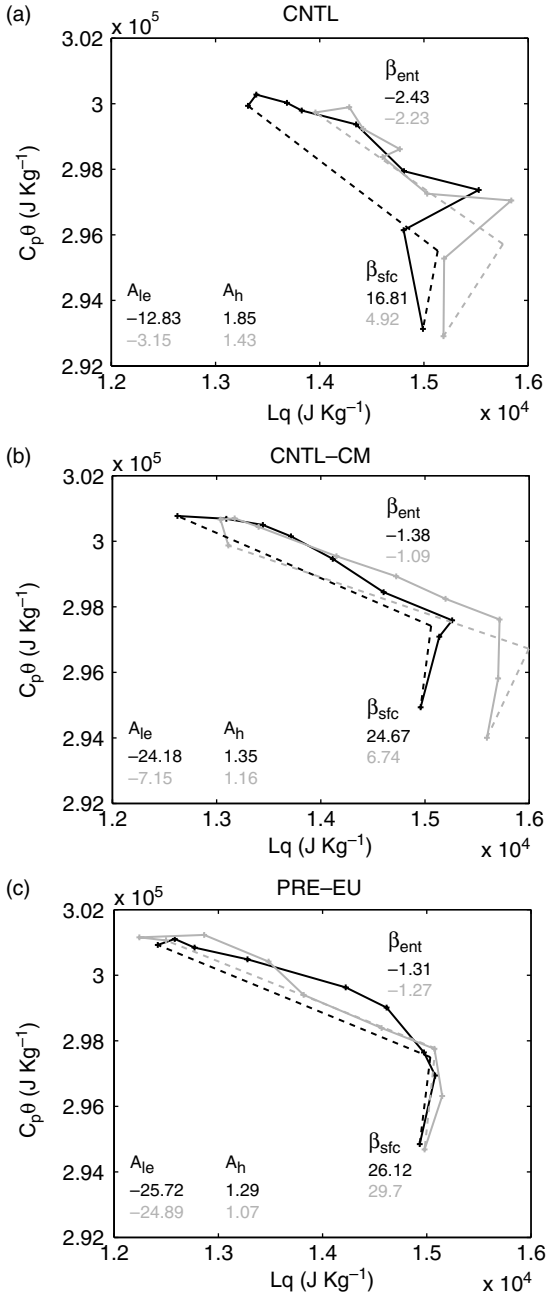

Figure 10. Same as in Figure 9, except on 21 August 2007.

Table 2. Surface (sfc) and entrainment (ent) fluxes (W m^{-2}) of heat (H) and moisture (LE) from the total mean flux (tot) and mean height (km) of the PBL (PBLH) for the the experiments in Table 1 for the 17 December 2005 case at the LKE and LKW sites.

	H_{tot}	H_{sfc}	H_{ent}	LE_{tot}	LE_{sfc}	LE_{ent}	PBLH
CNTL							
LKE	736.23	421.62	314.61	−90.66	8.07	−98.74	2.1
LKW	613.22	312.84	300.38	−66.50	19.06	−85.56	1.7
CNTL-CM							
LKE	749.53	415.65	333.88	−97.26	12.19	−109.45	2.2
LKW	665.12	309.98	355.14	−82.85	20.34	−103.19	1.8
PRE-EU							
LKE	834.12	428.14	405.98	−155.45	15.31	−170.76	2.3
LKW	813.91	430.63	383.28	−171.61	15.02	−186.63	2.2

Table 3. Same as in Table 2, except for the 21 August 2007.

	H_{tot}	H_{sfc}	H_{ent}	LE_{tot}	LE_{sfc}	LE_{ent}	PBLH
CNTL							
LKE	568.58	199.26	369.32	−140.23	11.86	−152.08	2.0
LKW	434.24	178.81	255.43	−78.10	36.32	−114.43	1.5
CNTL-CM							
LKE	545.08	231.92	313.17	−217.91	9.4	−227.32	2.2
LKW	422.63	195.80	226.82	−178.66	29.03	−207.69	1.9
PRE-EU							
LKE	567.78	248.05	319.74	−234.83	9.50	−244.32	2.2
LKW	549.30	265.62	283.68	−213.69	8.94	−222.63	2.1

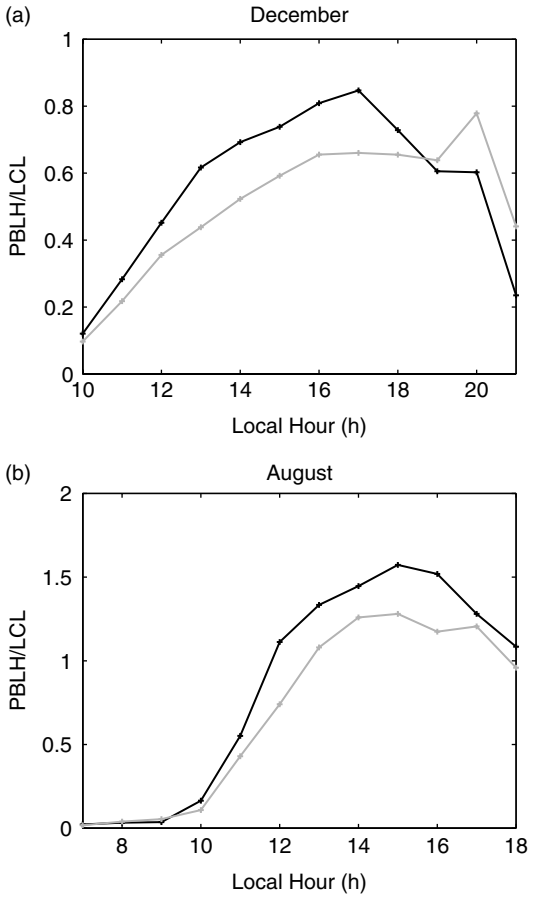

Figure 11. Ratio of PBLH to LCL for the CNTL experiments for (a) the August and (b) December case, respectively, at LKE (black) and LKW (grey).

change in land use and consequent increase in sensible heat flux drives the observed differences in PBL. On the case study days considered by Lyons (2002), air above the boundary layer was too moist for dry-air entrainment to occur, and Lyons (2002) argues that it was the higher sensible heat over the native vegetation which led to the formation of convective clouds. However, this study shows that even with dry-air entrainment occurring at both sites for the August case a higher surface Bowen ratio over the native vegetation can still lead to the preferential formation of convective clouds (Figure 6(a)). The PBL exceeds the LCL to a greater extent at the LKE site as compared to the LKW site, as illustrated in Figure 11(a). On the other hand, for the December case (Figure 11(b)), the PBL was higher at LKE compared to LKW, but did not exceed the LCL. Even under a drying climate, increased sensible heat flux over the darker native vegetation enhances cloud development. It is noted that the PBL is not only responsive to surface and entrainment fluxes but can also be influenced by differences in wind shear. However, observations showed no significant difference in wind shear between the two sites and, given the homogeneous initialization, this was also replicated in the simulations.

6. Conclusions

LES simulations are carried out using RAMS 6.0 to investigate the drivers behind higher PBL heights over native vegetation as compared to bare soil or crops observed from atmospheric soundings during specific case study days in December 2005 and August 2007 respectively. The model is initialized with the morning soundings and evaluated against the afternoon soundings, and shown to reproduce the observed differences in PBL well. Sensitivity tests are carried out with horizontally homogeneous soil moisture and pre-European vegetation, and it is found that the higher PBL heights over the native vegetation is mainly driven by the higher sensible heat fluxes over this region, due to the lower albedo and higher stomatal resistance of the wooded grasslands as compared to bare soil or crops. The enhanced PBL development over the native vegetation for the August case led to the formation of convective clouds with roll-like formations, similar to the idealized LES simulations of Esau and Lyons (2002). However, unlike Esau and Lyons (2002), whose grid domain was limited to 6 km and only focused on the effects of a sharp vegetation boundary, this study shows that the preferential formation over the native vegetation extends well east of the fence. The mixing diagram approach is applied to further quantify the relative contributions of surface *versus* entrainment fluxes, and it is found that while dry-air entrainment plays an important role in the growth of the PBL it is the surface fluxes which drive more vigorous PBL development over the native vegetation. In this semiarid environment, the removal of native vegetation has clearly reduced the development of the PBL by altering surface fluxes and consequently altered cloud dynamical processes. Hence this study further reinforces previous work which has shown that land cover change may be partly responsible for the decrease in precipitation in SWWA (Pitman *et al.*, 2004; Kala *et al.*, 2011; Nair *et al.*, 2011).

Acknowledgements

All RAMS simulations were supported by iVEC (http://www.ivec.org) through the use of advanced computing resources provided by the Australian Resources Research Centre Facility located at Technology Park, Perth. The radiosonde observations were acquired using the National Center for Atmospheric Research Mobile Global Positioning System Advanced Upper-Air Sounding System with support from the National Science Foundation Grant ATM 0523583 and the Australian Research Council's Discovery funding scheme (Project DP0664515). The Australian Water Availability Project (AWAP) soil moisture products were provided by Peter Briggs and Michael Raupach from the Commonwealth Scientific and Industrial Research Organisation division Marine and Atmospheric Research. Joseph A. Santanello Jr assisted in applying the mixing diagram theory to the simulations. Jatin Kala is supported by an Australian Post-Graduate Award at Murdoch University, Perth, Western Australia. The satellite imagery in Figure 7 was provided by Prof. Tokio Kikuchi, Kochi University, Japan. The comments of two anonymous reviewers helped improve the manuscript. All of this assistance is gratefully acknowledged.

References

Angevine WM, Jiang H, Mauritsen T. 2010. Performance of an eddy diffusivity-mass flux scheme for shallow cumulus boundary layers. *Mon. Weather Rev.* **138**: 2895–2912.

AUSLIG. 1990. *Atlas of Australian Resources: Vegetation*. Australian Surveying and Land Information Group: Canberra.

Avissar R, Schmidt T. 1998. An evaluation of the scale at which ground-surface heat flux patchiness affects the convective boundary layer using large eddy simulations. *J. Atmos. Sci.* **55**: 2666–2689.

Avissar R, Eloranta EW, Gürer K, Tripoli GJ. 1998. An evaluation of the large-eddy simulation option of the Regional Atmospheric Modeling System in simulating a convective boundary layer: a FIFE case study. *J. Atmos. Sci.* **55**: 1109–1130.

Betts AK. 1984. Boundary layer thermodynamics of a High Plains severe storm. *Mon. Weather Rev.* **112**: 2199–2211.

Betts AK. 1992. FIFE atmospheric boundary layer budget methods. *J. Geophys. Res.* **97**: 18523–18531.

Bohrer G, Katul GG,Walko RL, Avissar R. 2009. Exploring the effects of microscale structural heterogeneity of forest canopies using large-eddy simulations. *Boundary-Layer Meteorol.* **132**: 351–382.

Cheng WYY, Wu T, Cotton WR. 2001. Large-eddy simulations of the 26 November 1991 FIRE II cirrus case. *J. Atmos. Sci.* **58**: 1017–1034.

Cotton WR, Pielke RA, Walko RL, Liston GE, Tremback CJ, Jiang H, McAnelly RL, Harrington JY, Nicholls ME, Carrio GG, McFadden JP. 2003. RAMS 2001: current status and future directions. *Meteorol. Atmos. Phys.* **82**: 5–29.

Deardorff JW. 1980. Stratocumulus-capped mixed layers derived from a three-dimensional model. *Boundary- Layer Meteorol.* **18**: 495–527.

Doran JC, Shaw WJ, Hubbe JM. 1995. Boundary layer characteristics over areas of inhomogeneous surface fluxes. *J. Appl. Meteorol.* **34**: 559–571.

Eastman JL, Pielke RA, McDonald DJ. 1998. Calibration of soil moisture for large-eddy simulations over the FIFE area. *J. Atmos. Sci.* **55**: 1131–1140.

Ek MB, Holtslag AAM. 2004. Influence of soil moisture on boundary layer cloud development. *J. Hydrometeorol.* **5**: 86–99.

Esau IN, Lyons TJ. 2002. Effect of sharp vegetation boundary on the convective atmospheric boundary layer. *Agric. Forest Meteorol.* **114**: 3–13.

Findell KL, Eltahir EAB. 2003a. Atmospheric controls on soil moisture-boundary layer interactions: three-dimensional wind effects. *J. Geophys. Res.* **108**: 8385, DOI: 10.1029/2001JD001515.

Findell KL, Eltahir EAB. 2003b. Atmospheric controls on soil moisture–boundary layer interactions. Part I: Framework development. *J. Hydrometeorol.* **4**: 552–569.

Gentilli J. 1971. *Australian Climate Patterns*. Thomas Nelson (Australia): Melbourne.

Gopalakrishnan SG, Avissar R. 2000. An LES study of the impacts of land surface heterogeneity on dispersion in the convective boundary layer. *J. Atmos. Sci.* **57**: 352–371.

Gopalakrishnan SG, Roy SB, Avissar R. 2000. An evaluation of the scale at which topographical features affect the convective boundary layer using large eddy simulations. *J. Atmos. Sci.* **57**: 334–351.

Harrington JY. 1997. The effects of radiative and microphysical processes on simulated warm and transition season Arctic stratus. Atmospheric Science Paper 637. PhD thesis, Colorado State University.

Huang X, Lyons TJ. 1995. The simulation of surface heat fluxes in a land surface–atmosphere model. *J. Appl. Meteorol.* **34**: 1099–1111.

Huang X, Lyons TJ, Smith RCG. 1995. Meteorological impact of replacing native perennial vegetation with annual agricultural species. *Hydrol. Processes* **9**: 645–654.

Hutchinson MF, Stein JA, Stein JL. 2009. GEODATA 9 Second Digital Elevation Model (DEM-9S) Version 3. http://www.ga.gov.au/

Kala J, Lyons TJ, Nair US. 2011. Numerical simulations of the impacts of land-cover change on cold-fronts in southwest Western Australia. *Boundary-Layer Meteorol.* **138**: 121–138.

Li F, Lyons TJ. 2002. Remote estimation of regional evapotranspiration. *Environ. Model. Software* **17**: 61–75.

Lyons TJ. 2002. Clouds prefer native vegetation. *Meteorol. Atmos. Phys.* **80**: 131–140.

Lyons TJ, Schwerdtfeger P, Hacker JM, Foster IJ, Smith RCG, Huang X. 1993. Land–atmosphere interaction in a semiarid region: the bunny fence experiment. *Bull. Am. Meteorol. Soc.* **16**: 551–558.

Lyons TJ, Smith RCG, Huang X. 1996. The impact of clearing for agriculture on the surface energy balance. *Int. J. Climatol.* **16**: 551–558.

Nair US, Wu Y, Kala J, Lyons TJ, Pielke RA, Hacker JM. 2011. The role of land use change on the development and evolution of the west coast trough, convective clouds, and precipitation in Southwest Australia. *J. Geophys. Res.* **116**: D07103, DOI: 10.1029/2010JD014950.

Pielke RA, Cotton WR, Walko RL, Tremback CJ, Lyons WA, Grasso LD, Nicholls ME, Moran MD, Wesley DA, Lee TJ, Copeland JH. 1992. A comprehensive meteorological modelling system-RAMS. *Meteorol. Atmos. Phys.* **49**: 69–91.

Pitman AJ, Narisma GT, Pielke RA, Holbrook NJ. 2004. Impact of land cover change on the climate of southwest Western Australia. *J. Geophys. Res.* **109**: D18109, DOI: 10.1029/2003JD004347.

Raupach MR, Briggs PR, Haverd V, King EA, Paget M, Trudinger CM. 2008. Australian Water Availability Project. CSIRO Marine and Atmospheric Research, Canberra, Australia. http://www.csiro.au/awap

Raupach MR, Briggs PR, Haverd V, King EA, Paget M, Trudinger CM. 2009. *Australian Water Availability Project (AWAP): CSIRO Marine and Atmospheric Research Component: Final Report for Phase 3*. CAWCR Technical Report No. 013.

Ray DK, Nair US, Welch RM, Han Q, Zeng J, Su W, Kikuchi T, Lyons TJ. 2003. Effects of land use in Southwest Australia. 1. Observations of cumulus cloudiness and energy fluxes. *J. Geophys. Res.* **108**: 4414, DOI: 10.1029/2002JD002654.

Santanello JA, Friedl MA, Kustas WP. 2005. Am empirical investigation of convective planetary boundary layer evolution and its relationship with the land surface. *J. Appl. Meteorol.* **44**: 917–932.

Santanello JA, Friedl MA, Ek MB. 2007. Convective planetary boundary layer interactions with the land surface at diurnal time scales: diagnostics and feedbacks. *J. Hydrometeorol.* **8**: 1082–1097.

Santanello JA, Peters-Lidard CD, Kumar SV, Alonge C, Tao WK. 2009. A modeling and observational framework for diagnosing local land–atmosphere coupling on diurnal time scales. *J. Hydrometeorol.* **10**: 577–599.

Tian W, Parker DJ, Kilburn CAD. 2003. Observations and numerical simulation of atmospheric cellular convection over mesoscale topography. *Mon. Weather Rev.* **131**: 222–235.

van Heerwaarden CC, de Arellano JVG, Moene AF, Holtslag AAM. 2009. Interactions between dry-air entrainment, surface evaporation and convective boundary-layer development. *Q. J. R. Meteorol. Soc.* **135**: 1277–1291.

Walko RL, Tremback CJ. 2006. *RAMS – Regional Atmospheric Modelling System Version 6.0*. Model input namelist parameters. Document Edition 1.4.

Walko RL, Band LE, Baron J, Kittel TGF, Lammers R, Lee TJ, Ojima D, Pielke RA, Taylor C, Tague C, Tremback CJ, Vidale PL. 2000. Coupled atmosphere–biosphere hydrology models for environmental modeling. *J. Appl. Meteorol.* **39**: 931–944.

Wang C, Tian W, Parker DJ, Marsham JH, Guo Z. 2010. Properties of a simulated convective boundary layer over inhomogeneous vegetation. *Q. J. R. Meteorol. Soc.* **137**: 99–117.

